WALAILAK JOURNAL
Applied Sciences
http://wjst.wu.ac.th https://doi.org/10.48048/wjst.2021.21424

Analysis of Platelet Shape Al_2O_3 and TiO_2 on Heat Generative Hydromagnetic Nanofluids for the Base Fluid $C_2H_6O_2$ in a Vertical Channel of Porous Medium

Silpi HAZARIKA[1], Sahin AHMED[1,*] and Ali J. CHAMKHA[2]

[1]Heat Transfer and Fluid Mechanics Research, Department of Mathematics,
Rajiv Gandhi University, Arunachal Pradesh 791112, India
[2]Faculty of Engineering, Kuwait College of Science and Technology, Doha District, Kuwait

([*]Corresponding author's email: nanofluid.sahin@gmail.com)

Received: 4 February 2021, Revised: 30 April 2021, Accepted: 5 May 2021

Abstract

An analytical investigation is performed on the unsteady hydromagnetic flow of nanoparticles Al_2O_3 and TiO_2 in the EG base fluid through a saturated porous medium bounded by two vertical surfaces with heat generation and no-slip boundary conditions. The physics of initial and boundary conditions is designated with the flow model's non-linear partial differential equations. The analytical expressions of nanofluid velocity and temperature with the channel are derived, and Matlab Codes are used to plot the significant results for physical variables. From the physical point of view for nanofluid velocity and temperature results, the base fluid $C_2H_6O_2$ has a higher viscosity and thermal conductivity than that of water. Physically, the platelet shape Al_2O_3 nanofluid has the highest velocity than TiO_2 nanofluid. It is found that the velocity of nanofluid enhanced the porosity and nanoparticles volume fraction for Al_2O_3 - EG and TiO_2 - EG base nanofluids. However, this trend is reversed for the effects of heat generation. Obtained results indicate that an increase in nanoparticles volume fraction raises the skin friction near the surface, but profiles gradually become linear, due to less frictional effects of nanoparticles. Moreover, due to higher values of nanoparticles volume fraction, the thermal conductivity is raised, and thus the thickness of the thermal boundary layer is declined. The results show that the method provides excellent approximations to the analytical solution of nonlinear system with high accuracy. Metal oxide nanoparticles have wide applications in various fields due to their small sizes, such as the pharmaceutical industry and biomedical engineering.

Keywords: Aluminium oxide, Ethylene Glycol, Heat generation, Hydromagnetic boundary layer flow, Porosity, Nanoparticles volume fraction, Titanium dioxide

Introduction

The interest in nanofluids has increased due to their indispensable role in various industrial applications since they play a vital role in enhancing the heat transfer performance compared to pure liquids. Thus, they can be considered the most exciting heat transfer fluids. Given the properties of thermal enhancement, nanofluids may be used for the cooling systems such as motion over flat plates or in Couette and Poisueille flow, for which many researchers have analyzed heat transfer over different surfaces. Alumina and Titanium dioxide nanoparticles are widely used in various sectors of everyday life. They are utilized in fire retard, insulator, surface protective coating, reducing toxicity of dyes, pharmaceutical drugs, space applications, food industries and many other.

Choi [1] conducted a pioneer investigation on nanoparticles that a small number of nanoparticles in the base fluid may increase the rate of thermal conductivity and their convective heat transfer. Generally, the most favourable nanoparticles are Copper, Silver, Aluminium, Titanium dioxide, CNT's, various oxides, while the common base fluids are water, ethylene glycol, oils, and polymer solutions. However, the thermal conductivity of nanoparticles depends on their size and shape, and physically the thermal conductivity of nanoparticles is heavier than the base fluids. The pioneering work of anomalous increases in nanofluids' thermal conductivity has become the topic of much research. Other potentially useful properties of nanofluids have also been discussed extensively through further experimental and numerical research that will help to develop a better understanding of nanofluid flows and their heat transfer properties. In 1873, Maxwell [2] studied one of the first theoretical investigations regarding effective thermal conductivity and electroism. Mahdi *et al*. [3] reviewed the nanofluid flow and heat transfer through porous media. First, they studied the main characteristics of a porous medium: porosity, permeability, and effective thermal conductivity. They analyzed the works with the emphasis on the thermophysical properties of the nanofluid and the type of convection heat transfer. Nasrin *et al*. [4] discussed the forced convection in a channel with a porous medium filled with nanofluid.

Studying the magnetic field in nanofluid is also an interesting topic in Science and Engineering applications, particularly polymer industry and metallurgy. Wubshet and Bandari [5] presented the study of nanofluid with the effects of the magnetic field, slip boundary condition, and thermal radiation over a permeable stretching sheet. They noticed that the velocity profiles decreases with increasing magnetic parameter. Nanofluid technology radiation effect helps to perform free convection with the consideration of magnetic field, and a gradual decrement in heat transfer was obtained by Sheikholeslami [6] in the presence of Lorentz forces. They also studied a heat transfer that is force convective with magnetic nanofluid flow [7]. Awan *et al*. [8] studied numerical treatment on the dynamical analysis of hydro-magnetic nanofluids problem for heat and mass transfer of an unsteady nanofluid flow between parallel plates by exploiting the strength of Adams and explicit Runge-Kutta method. Akula and Srinivas [9] investigated the hydromagnetic pulsating nanofluid flow in a porous channel with thermal radiation. In this work, they considered water as the base fluid and silver (Ag), copper (Cu), alumina (Al_2O_3) and titanium dioxide (TiO_2) as nanoparticles. Malavandi and Ganjii [10] have made a theoretical investigation on mixed convective aluminium oxide nanoparticles in a vertical channel of flow with wall heat fluxes, and they considered water as base fluid. Sheikholeslami *et al*. [11] have obtained analytical solutions from the effect of magnetic forces in a porous channel of nanofluids.

The quality of nanofluid depends on the type of nanoparticles and their shapes [12]. Today, researchers have a keen interest in studying their spherical shapes. Our study also deals with four different types of nanoparticles namely cylinder, platelet, blade, and brick. Various recent investigations show that cylindrical shaped nano-particles are more deadly than other spherical shaped nanoparticles. Volume fraction is studied by Jang *et al*. [13], who explained that effective thermal conductivity of nanofluid increases with increasing volume fraction of the nanoparticles. This confirms that it is more effective to use small volume fractions in nanofluids. Widodo *et al.* [14] discussed the MHD nanofluid flow through a porous cylinder and they noted that an increment in the nanoparticle volume fraction cause an increment in the temperature profile but decrement in the velocity profile. Hamilton and Croser [15] studied the effectiveness of the thermal conductivity in heterogeneous systems. Likewise, Timofeeva *et al*. [16] have extended their research for different shaped nanoparticles in Al_2O_3 nanofluid. Similar works have been done by many researchers [17, 18] with various sizes and shapes of nanoparticles over flat plate/channel with heat transport for suitable conditions. The investigation on nanofluid with special emphasis on thermal radiation over a porous vertical cylinder is done by Kabeir *et al*. [19].

Hazarika *et al*. [20,21] investigated the behaviour of CNT's in a vertical channel for human blood flow and Casson fluid. Hazarika *et al*. [22] developed a numerical solution through finite difference scheme for the impact of thermophoresis and dissipating heat on hydromagnetic fluid over a stretching sheet in presence of nanoparticles Cu, Ag and Fe_3O_4. The importance of three nanoparticles is found in medical industry and biocompatibility engineering. Hazarika *et al*. [23] presented a theoretical investigation of diffusion-thermo on a chemically reacting hydro-magnetic flow of Cu-water nanofluid over a semi-infinite vertical surface in a porous medium, and augmented values of flow velocity are detected for Cu-nanofluid than the water-base fluid for the impact of diffusion-thermo. Armaghani *et al*. [25] numerically presented the impact of natural convection heat transfer and entropy generation of water-alumina nanofluid in baffled L-shaped cavity. The influence of the heat sink, the heat source and the entropy generation on MHD mixed convection flow in a porous enclosure filled with a Cu-water nanofluid was deliberated by Chamkha *et al*. [26]. Molana *et al*. [27] presented the cavity filled by Fe_3O_4-water nanofluid and its shape associated with porous medium and natural convection under a constant inclined magnetic field. Futher, Armaghani *et al*. [28] analyzed the entropy generation in an inclined partially porous layered cavity filled with a nanofluid and observed that for minimum value of Rayleigh number, porous layer thickness is higher and also for higher cavity orientation, the thermal performance is increased

Hybrid nanofluid delivers a higher heat transfer rate than the nanofluids. Recently, the study of hybrid nanofluid with different physical parameter becomes the theme of active research. Rashad *et al*. [29] studied the effect of hybrid nanofluid's volume fraction considering minimum natural convection. Jakeer *et al*. [30] discussed magneto Cu-Al_2O_3/water hybrid nanofluid flow in a non-Darcy porous square cavity and found that the Cu-Al2O3/water nanofluid provides a higher heat transfer. MHD convective flow of water-based hybrid-nanofluid containing Alumina and Copper nanoparticles through a horizontal circular cylinder was studied by Zahar *et al*. [31]. Futhermore, Ghalambaz *et al*. [32] investigated nano encapsulated phase change material in a glass ball porous medium, where the nanoparticles comprise of PCM core (nonadecane) and a shell (polyurethane). Extending this work, Zadeh *et al*. [33] presented the thermal and hydrodynamic effect with entropy generation for nano encapsulated phase change material.

The novelty of the present model is to investigate the outcomes drawn from the platelet-shaped nanoparticles in a Couette flow as well as Poiseuille flow in the presence of magnetic forces, thermal radiation, and heat generation subject to no-slip condition at the plates. An infinite series solution tool has been adopted to analyze the fluid variables within the boundary layer. The important behaviour of the variables such as porosity, magnetic drag force, heat generation, and nanoparticle volume fraction over the nanofluid velocity and temperature in Couette and Poiseuille flow is highlighted. During the investigation, the nanoparticles of Aluminium oxide and Titanium dioxide are added to the base fluid Ethylene Glycol and compared the impact of the produced nanofluid for the velocity, temperature, and skin friction profiles.

Mathematical formulation

In this investigation, a vertical channel flow of electrically conducting nanofluid contains Aluminium oxide and Titanium dioxide. The channel is immersed in a saturated porous medium in presence of thermal radiation, and heat generation is presented in **Figure A**. The co-ordinate axes $\overline{\zeta}$ and $\overline{\xi}$ are displayed along and normal to the surface $\overline{\xi} = 0$ respectively, where $(\overline{\psi}, \overline{\chi})$ are the velocity components in the direction of $(\overline{\zeta}, \overline{\xi})$. Transverse magnetic field of constant strength H_0 is applied to the planes of the channel. In Couette flow, the plate $\overline{\xi} = d$ is oscillating with the velocity $\overline{\psi}(\overline{d}, \overline{t}) = \varepsilon\, \overline{H}(\overline{t})\, e^{i\overline{\omega}\overline{t}}$, while both the plates are stationary in Poiseuille flow.

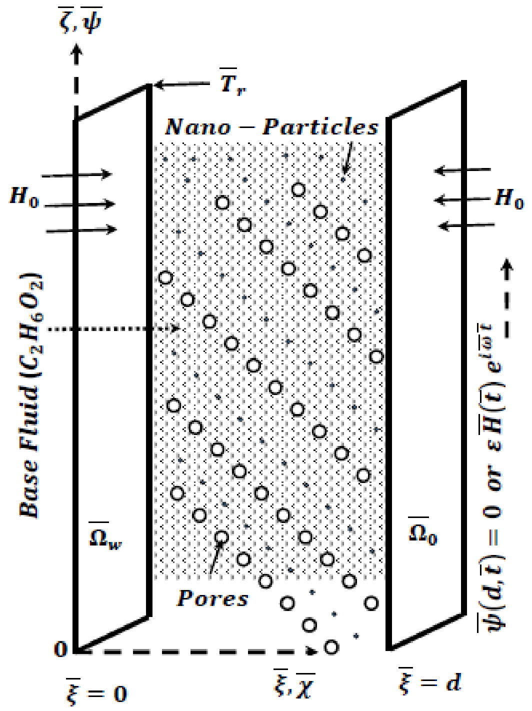

Figure A Geometry of flow model.

The Navier-Stokes equation and energy equation for this channel flow of nanofluid under the usually Boussinesq approximation are [21,22]:

$$\overline{\chi}_{\overline{\xi}} = 0\,, \tag{1}$$

$$\rho_{nf}\left(\overline{\psi}_{\overline{t}}\right) = -\overline{p}_{\overline{\zeta}} + \mu_{nf}\, \overline{\psi}_{\overline{\xi}\,\overline{\xi}} + (\rho\beta)_{nf}\, g\left(\overline{\Omega} - \overline{\Omega}_0\right) - \left(\sigma H_0^2 + \mu_{nf}\overline{K}_1^{-1}\right)\overline{\psi}\,, \tag{2}$$

$$\left(\rho C_p\right)_{nf}\left(\overline{\Omega}_{\overline{t}}\right) = \kappa_{nf}\, \overline{\Omega}_{\overline{\xi}\,\overline{\xi}} - \left(\overline{T}_r\right)_{\overline{\xi}} - Q_g\left(\overline{\Omega} - \overline{\Omega}_0\right), \tag{3}$$

The thermal conductivity [15] and dynamic viscosity [16] for different shapes of nanoparticles are as;

$$\left\{\begin{matrix} n=\frac{3}{\Delta},\ \mu_{nf}=\mu_f\,(1+a\phi+b\phi^2),\ (\rho)_{nf}=(1-\phi)(\rho)_f+\phi(\rho)_s, \\ (\rho\beta)_{nf}=(1-\phi)(\rho\beta)_f+\phi(\rho\beta)_s,\ (\rho C_p)_{nf}=(1-\phi)(\rho C_p)_f+\phi(\rho C_p)_s, \\ \frac{\kappa_{nf}}{\kappa_f}=\frac{\kappa_s+(n-1)\kappa_f+(n-1)(\kappa_s-\kappa_f)\phi}{\kappa_s+(n-1)\kappa_f-(\kappa_s-\kappa_f)\phi} \end{matrix}\right\} \tag{4}$$

Due to thermal radiating flow, the heat flux is defined as [21],

$$(\overline{T}_r)_{\overline{\xi}}=-4\alpha^2(\overline{\Omega}-\overline{\Omega}_0) \tag{5}$$

The non-dimensional parameters are:

$$\left\{\begin{matrix} \zeta=\frac{\overline{\zeta}}{d},\ \xi=\frac{\overline{\xi}}{d},\ \psi=\frac{\overline{\psi}}{U_0},\ t=\frac{\overline{t}\,U_0}{d},\ \nu_f=\frac{\mu_f}{\rho_f},\ K_P=\frac{\overline{K}_1}{d^2},\ \lambda_n=\frac{\kappa_{nf}}{\kappa_f}, \\ \Omega=\frac{\overline{\Omega}-\overline{\Omega}_0}{\overline{\Omega}_w-\overline{\Omega}_0},\ p=\frac{\overline{p}d}{\mu\,U_0},\ \omega=\frac{\overline{\omega}d}{U_0},\ \frac{\partial p}{\partial x}=\lambda e^{i\omega t},\ P_e=\frac{U_0 d(\rho C_p)_f}{k_f}, \\ R_e=\frac{U_0 d}{\nu_f},\ M_d^2=\frac{\sigma d^2 H_0^2}{\mu_f},\ G_h=\frac{d^2 g\beta_f(T_w-T_0)}{U_0\mu_f},\ T_r^2=\frac{4d^2\alpha^2}{\kappa_f},\ H_g=\frac{d^2Q_g}{\kappa_{nf}} \end{matrix}\right\} \tag{6}$$

With the help of (4) - (6), Eqs. (2) - (3) reduce to the dimensionless form:

$$\phi_1 R_e(\psi_t)=\varepsilon\lambda\,e^{i\omega t}+\phi_2(\psi_{\xi\,\xi})-M_d^2\psi-\phi_2 K_P^{-1}\psi+\phi_3 G_h\,\Omega \tag{7}$$

$$\phi_4 P_e\,\lambda_n^{-1}\,(\Omega_t)=(\Omega_{\xi\,\xi})+T_r^2\lambda_n^{-1}\Omega-H_g\Omega \tag{8}$$

We have studied 2 cases that are related to Poiseuille flow and Couette flow motion for the behaviour of nanoparticles in EG base fluid.

Poiseuille flow motion (When both the channel walls are stationary)

The boundary conditions are [20, 21],

$$\left\{\begin{matrix} \overline{\psi}(0,t)=0,\ \overline{\psi}(d,t)=0 \\ \overline{\Omega}(0,t)=\overline{\Omega}_0,\ \overline{\Omega}(d,t)=\overline{\Omega}_\infty \end{matrix}\right\} \tag{9}$$

The dimensionless forms of (9) are,

$$\left\{\begin{matrix} \psi(0,t)=0,\ \psi(1,t)=0 \\ \Omega(0,t)=0,\ \Omega(1,t)=1 \end{matrix}\right\}\ t>0$$

The Eqs. (6) and (7) may be re-written as,

$$a_0\psi_t=\varepsilon\lambda e^{i\omega t}+\phi_2\psi_{\xi\xi}-m_0^2\psi+a_1\Omega \tag{10}$$

$$b_0^2\,\Omega_t=\Omega_{\xi\xi}+(b_1^2-H_g)\Omega \tag{11}$$

Basically, the Perturbation scheme is to formulate the desired solution in terms of a power series which can be expanded in a small parameter that computes the deviation from the exact solution of the problem. In this powerful series, the first term is considered as the exact solution of the problem with zeroth order. In contrast, further terms describe the deviation in the solution due to the deviation from the initial problem.

When the flow problem is to be expressed by adding a "small" term (In this work, ε perturbation constant) to the mathematical description for the exact solution, then this theory can be relevant.

The infinite series solution tools is to apply for the analytical solutions o Eqs. (10) - (11) and are defined as;

$$\left\{\begin{aligned}\psi(\xi,t) &= \psi_0(\xi) + \sum_{j=1}^{\infty} \varepsilon^j\, e^{i\omega t}\psi_j(\xi) \\ \Omega(\xi,t) &= \Omega_0(\xi) + \sum_{j=1}^{\infty} \varepsilon^j\, e^{i\omega t}\Omega_j(\xi)\end{aligned}\right\} \text{ where } 0 < \varepsilon \ll 1 \tag{12}$$

The formulation (12) is called the classical perturbation scheme, which is a convergent scheme due to $\varepsilon \ll 1$ and so the higher order terms may be omitted. Through this technique, Eqs. (10) - (11) are transformed into ordinary differential equations;

$$\frac{d^2\psi_0(\xi)}{d\xi^2} - m_1^2\psi_0(\xi) = -a_2\Omega_0(\xi)\,, \tag{13}$$

$$\frac{d^2\psi_1(\xi)}{d\xi^2} - m_2^2\psi_1(\xi) = -\lambda_1 - a_2\Omega_1(\xi)\,, \tag{14}$$

$$\frac{d^2\Omega_0(\xi)}{d\xi^2} + b_2^2\Omega_0(\xi) = 0\,, \tag{15}$$

$$\frac{d^2\Omega_1(\xi)}{d\xi^2} + b_3^2\Omega_1(\xi) = 0\,, \tag{16}$$

The reduced boundary conditions are;

$$\left\{\begin{matrix}\psi_0(0) = 0\,, & \psi_0(1) = 0\,, & \psi_1(0) = 0\,, & \psi_1(1) = 0 \\ \Omega_0(0) = 0\,, & \Omega_0(1) = 1\,, & \Omega(0) = 0\,, & \Omega_1(1) = 0\end{matrix}\right\} \tag{17}$$

The solutions of the Eqs. (13) - (16) the under boundary conditions (17) yield to;

$$\Omega(\xi,t) = \frac{sinb_2\xi}{sinb_2} \tag{18}$$

$$\psi(\xi,t) = \begin{bmatrix} \dfrac{a_2}{(b_2^2 + m_1^2)}\left\{-\dfrac{sinh(m_1\xi)}{sinhm_1} + \dfrac{sin(b_2\xi)}{sinb_2}\right\} \\ + \varepsilon\, e^{i\omega t}\left\{\dfrac{\lambda_1(coshm_2 - 1)}{m_2^2\, sinhm_2} sinh(m_2\xi) - \dfrac{\lambda_1}{m_2^2}(cosh(m_2\xi) - 1)\right\}\end{bmatrix} \tag{19}$$

Couette flow motion (When the plate $\bar{\xi} = \mathbf{d}$ of the channel is oscillating)

The boundary conditions for the flow velocity $\bar{\psi}(\bar{\xi},\bar{t})$ are;

$$\bar{\psi}(0,\bar{t}) = 0, \bar{\psi}(d,\bar{t}) = \varepsilon\, \bar{H}(\bar{t})\, e^{i\,\bar{\varpi}\,\bar{t}}, \tag{20}$$

The non-dimensional forms of (20) is;

$$\psi(0,t) = 0,\ \ \psi(1,t) = \varepsilon\, H(t)\, e^{i\,\omega\,t};\ t > 0 \tag{21}$$

The transformed boundary conditions are;

$$\{\psi_0(0) = 0\ \ ,\ \ \psi_0(1) = 0\ \ ,\ \ \psi_1(0) = 0\ ,\ \ \psi_1(1) = H(t)\} \tag{22}$$

In view of (22), the analytical expression of the nanofluid velocity, $\psi(\xi,t)$ is;

$$\psi(\xi,t) = \begin{bmatrix} \dfrac{a_2}{(b_2^2 + m_1^2)}\left\{-\dfrac{sinh(m_1\xi)}{sinhm_1} + \dfrac{sin(b_2\xi)}{sinb_2}\right\} \\ +\,\varepsilon\, e^{i\omega t}\begin{Bmatrix} \dfrac{sinh(m_2\xi)}{sinhm_2}\{H(t) + \dfrac{\lambda_1}{m_2^2}(cosh\, m_2 - 1)\} \\ -\dfrac{\lambda_1}{m_2^2}(cosh(m_2\xi) - 1) \end{Bmatrix} \end{bmatrix} \tag{23}$$

Skin friction

In non-dimensional form, the shear stress (τ) at the surface $\xi = 0$ due to Poiseuille flow motion is;

$$\tau = \left[\frac{\partial\psi}{\partial\xi}\right]_{\xi=0} = \frac{a_2}{(b_2^2+m_1^2)}\left\{\frac{-m_1}{sinhm_1} + \frac{b_2}{sinb_2}\right\} + \varepsilon exp(i\omega t)\left[\frac{\lambda_1\{coshm_2-1\}}{m_2 sinhm_2}\right]$$

The shear stress (τ) at the surfaces $\xi = 0,1$ due to Couette flow motion in non-dimensional form are;

$$\tau = \left[\frac{\partial\psi}{\partial\xi}\right]_{\xi=0} = \begin{bmatrix} \dfrac{a_2}{(b_2^2+m_1^2)}\left\{\dfrac{-m_1}{sinhm_1} + \dfrac{b_2}{sinb_2}\right\} \\ +\varepsilon\, exp(i\omega t)\left\{\dfrac{m_2}{sinhm_2}\{H(t) + \dfrac{\lambda_1}{m_2^2}(cosh\, m_2 - 1)\}\right\} \end{bmatrix}$$

$$\tau = \left[\frac{\partial\psi}{\partial\xi}\right]_{\xi=1} = \begin{bmatrix} \dfrac{a_2}{(b_2^2+m_1^2)}\left\{\dfrac{-m_1 coshm_1}{sinhm_1} + \dfrac{b_2 cosb_2}{sinb_2}\right\} \\ +\varepsilon\, exp(i\omega t)\left\{\dfrac{m_2 coshm_2}{sinhm_2}\{H(t) + \dfrac{\lambda_1}{m_2^2}(cosh\, m_2 - 1)\} - \dfrac{\lambda_1}{m_2^2}\{m_2 sinh\}\right\} \end{bmatrix}$$

Validity and accuracy

To check the accuracy of the present nanofluid model, comparisons of the velocity and temperature of nanofluids have been conducted with published results obtained by the analytical method for different conditions: [18] at $H_g = 0$ and $K_P = 1$. The comparisons are presented in **Tables 1** and **2**. A very good agreement between the present and the other results confirms the accuracy of the method used. The present outcomes are compared with the foregoing ones, and an outstanding agreement is initiated between the current and previous results. The results obtained for velocity and temperature profiles through analytically have also been weighted up in the **Tables 1** and **2**, respectively, which clearly reflects the convergence of the perturbation method. It has been seen that the increasing values of ϕ declines velocity of nanofluids and temperature due to viscosity increases.

Table 1 Velocity distribution for ϕ in Al_2O_3 - EG based nanofluids at $\lambda = 1, \omega = 0.2, T_r = 0.1$, $G_h = 0.1$ due to Poiseuille flow (plates of the channel are stationary).

	Aaiza *et al.*[18] at $H_g = 0, K_P = 1$		**Aaiza *et al.* [18] at $H_g = 5, K_P = 1$**		**Present work at $H_g = 5, K_P = 1$**	
Y	ϕ = **0.01**	ϕ = **0.03**	ϕ = **0.01**	ϕ = **0.03**	ϕ = **0.01**	ϕ = **0.03**
0.0	0	0	0	0	0	0
0.2	0.00610346	0.00385615	0.00561805	0.00391052	0.00602841	0.00396063
0.4	0.00963398	0.00592734	0.00970170	0.00581105	0.00953183	0.00572347
0.6	0.01036501	0.00660882	0.00947011	0.00671250	0.00983020	0.00601821
0.8	0.00757679	0.00522940	0.00640118	0.00540711	0.00717823	0.00518347
1.0	0	0	0	0	0	0

Table 2 Temperature distribution for ϕ in Al_2O_3 -water based nanofluids at $\lambda = 0.5, \omega = 0.5, \Lambda = 0.52$, $T_r = 3$.

	Aaiza *et al.* [18] at $H_g = 0$			Present work **at $H_g = 5$**		
Y	ϕ = **0.02**	ϕ = **0.03**	ϕ = **0.04**	ϕ = **0.02**	ϕ = **0.03**	ϕ = **0.04**
0.0	0	0	0	0	0	0
0.2	0.00610346	0.00454687	0.00385615	0.00514568	0.00362057	0.00296063
0.4	0.00963398	0.00705224	0.00592734	0.00802538	0.00549658	0.00442347
0.6	0.01036501	0.00775816	0.00660882	0.00866330	0.00611265	0.00501821
0.8	0.00757679	0.00596958	0.00522940	0.00645758	0.00488739	0.00418347
1.0	1	1	1	1	1	1

Table 3 The values of *a* and *b* for Empirical shape factor.

Model	Platelet	Blade	Cylinder	Brick
A	37.1	14.6	13.5	1.9
B	612.6	123.3	904.4	471.4

Table 4 The values of Sphericity (Λ for different shapes of nanoparticles.

Model	Platelet	Blade	Cylinder	Brick
Λ	0.52	0.36	0.62	0.81

Table 5 Thermo-physical properties of base fluids and nanoparticles.

Sample	ρ (kgm^{-3})	C_p ($kg^{-1}K^{-1}$)	κ ($wm^{-1}k^{-1}$)	β ·10^{-5} (K^{-1})
H_2O	997.1	4179	0.618	21
$C_2H_6O_2$	1.115	0.58	0.1490	6.5
Cu	8933	385	401	1.67
TiO_2	4250	686.2	8.9528	0.9
Ag	10500	235	429	1.89
Al_2O_3	3970	765	40	0.85
Fe_3O_4	5180	670	9.7	0.5

Results and discussions

In this section, we deal with the theoretical and graphical behavior of nanoparticles along with different physical quantities that are obtained in the present flow problem. The computational software *Matlab* code has been utilized to investigate the novelties of all the physical parameters. In particular, we investigate the influence of various embedded parameters on velocity profiles, temperature profiles, and shear stress profiles of nanoparticles. The graphical explanation of these parameters has been displayed in **Figures 1 - 13**. Throughout the discussions, all the numerical calculations are done in the case of a platelet shape nanoparticles Al_2O_3 and TiO_2 in EG base fluids.

The nanofluid velocity and temperature distributions in case of Poiseuille flow motion (plates $\xi = 0$ and $\xi = 1$ are stationary) are displayed in **Figures 1 - 4** with $\phi = 0.01, R_e = 1, \varepsilon = 0.001, P_e = 1, K_P = 1, t = 2, H_g = 5, \lambda = 1, T_r = 0.1, M_d = 2, G_h = 0.1, \omega = 0.2$.

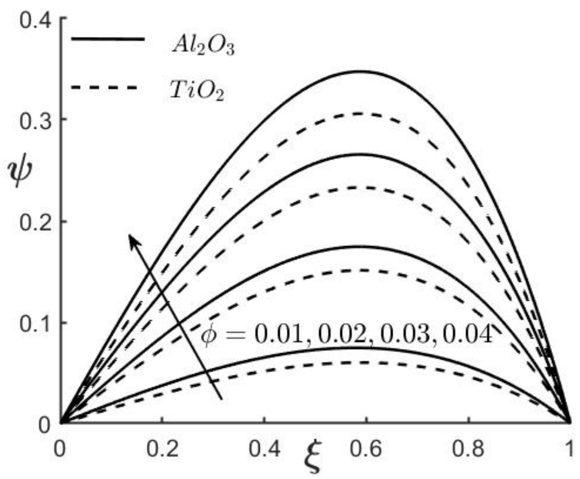

Figure 1 Effects of ϕ on Velocity distribution for Al_2O_3 and TiO_2.

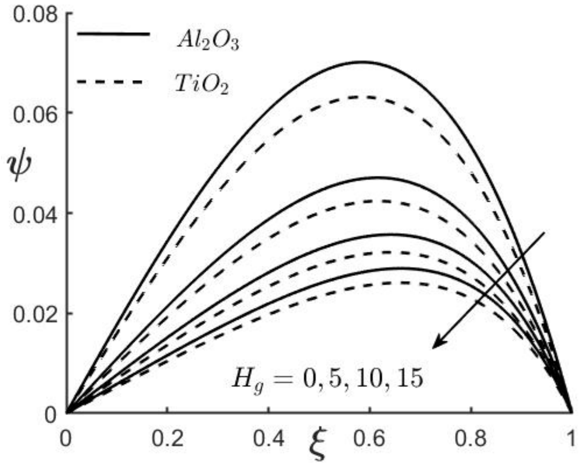

Figure 2 Effects of H_g on Velocity distribution for Al_2O_3 and TiO_2 .

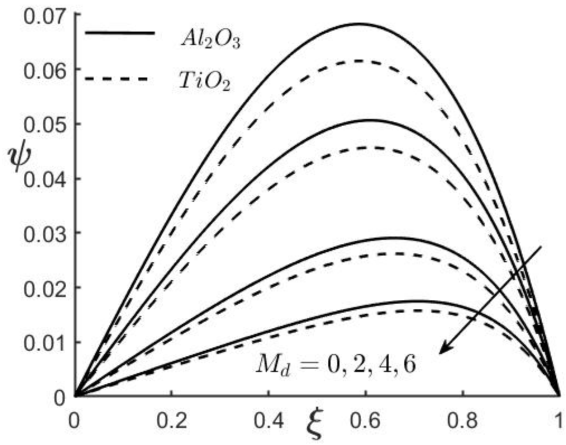

Figure 3 Effects of M_d on Velocity distribution for Al_2O_3 and TiO_2 in EG base fluid.

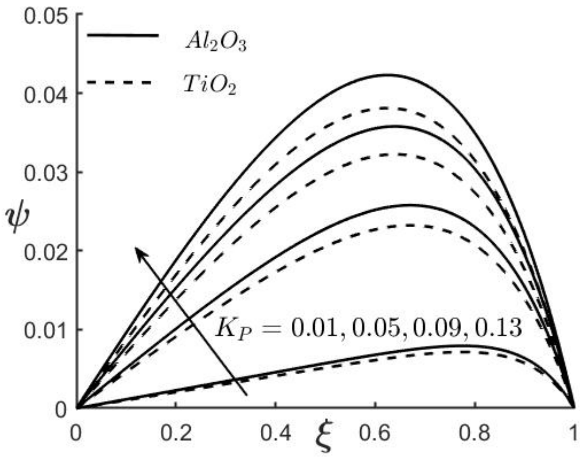

Figure 4 Effects of K_P on Velocity distribution for Al_2O_3 and TiO_2 in EG base fluid.

Figure 1 shows that the effect of nanoparticle volume fraction parameter (ϕ) on the nanoufluids velocity profiles, in the case of a platelet shape of Al_2O_3 and TiO_2 in EG base fluids. In nano technology, the nanoparticles volume fraction is the volumetric concentration of the nanoparticles in the fluid. It concurs with the volume concentration in ideal solutions where the volume of the solution is equal to the sum of the volumes of its constituents. It is observed that the velocity of the nanofluid upsurges when the nanoparticle volume fraction (ϕ) rises, because the fluid becomes more non-viscous with the growth of ϕ, which accelerates the nanofluid velocity. As platelet shape Al_2O_3 Nanofluids has the highest viscosity and the thermal conductivity compared to TiO_2, the nanofluid velocity (ψ) in the case of a TiO_2 - EG nanofluid is higher than that of Al_2O_3 - EG nanofluid. With an increasing nanoparticle volume fraction, the velocity boundary layer thickness increases for both types of nanofluids. This acquired result satisfies the experimental result obtained by Colla *et al.* [24].

Figure 2 shows the effect of heat generation (H_g) on the velocity of nanofluid in presence of Al_2O_3 and TiO_2 added to the base fluid EG. It can be seen that the increasing values of heat generation parameter reduce velocity curves. The term $Q_g\left(\overline{\Omega}-\overline{\Omega}_0\right)$ in the energy equation (3) represents the amount of heat generation or absorption per unit volume, where $Q_g > 0$ represents source or generation and $Q_g < 0$ represents sink. The nanoparticle Al_2O_3 has greater thermal conductivity $(\kappa \approx 430)$ which generates more heat than that of nanoparticle TiO_2 of thermal conductivity $(\kappa \approx 9)$, thereby velocities are overshoot for the nanoparticle Al_2O_3. A good variation also can be seen in these figures because of the heat generation $(H_g > 0)$ parameter. This is due to the fact that the presence of heat generation diminishes the momentum boundary layer thickness.

The variation of M_d over the velocity of nanofluid for presence of the nanoparticles Al_2O_3 and TiO_2 in base fluid EG is illustrated in **Figure 3**. The Hartmann number (M_d) is defined as the ratio of electromagnetic force to the viscous force and was introduced by Hartmann [35] to describe his experiments with viscous MHD channel flow. The magnitude of Hartmann number indicates the relative effects of magnetic and viscous drag. For the lower value of M_d, the Lorentz force is very small and it implies the low or moderate conductivities of the fluid. Therefore, the application of magnetics drag force always resists the motion of the molecules of base fluid and therefore, the movement of the molecules become slow in the prescribed channel. In addition, it is noted that in absence of the magnetic field $(M_d = 0)$, the curves of TiO_2 nanoparticles have more elevation due to low thermal conductivity than that of Al_2O_3 nanoparticles, and they have opposite characters for higher magnetic field $(M_d = 2, 4, 6)$. It is also observed that the motion of the molecules of nanofluid towards the surfaces are least due to magnetic resistive forces, while the free motion of molecules is seen in the middle of the channel.

Figure 4 shows the effects porosity (K_P) over the velocity of platelet shaped nanoparticles Al_2O_3 and TiO_2 in the base fluid EG. Physically, K_P is the measurement of void spaces in a material and it can be termed as $K_P =$ (volume of pores) / (volume of bulk solid bodies) and is usually expressed as a percentage. Porosity = (Volume of Voids / Total Volume) x 100 %. In this investigation, the porosity is based on Darcy's law after the name of H. Darcy [34]. In presence of the resistive forces of porosity, the friction of molecules in nanofluid gradually become lesser and hence the movement of the molecules enhances the flow velocity within the channel. Moreover, the friction of forces in the motion of Al_2O_3 in EG based nanofluids is heavier than that of TiO_2. These results find wider applications in the field of transportation engineering and cooling in commercial sectors.

The nanofluid velocity distributions in case of Couette flow motion (oscillating plate $\xi = 1$) are displayed in **Figures 5 - 11** with $\phi = 0.01, \varepsilon = 0.001, \lambda = 1, \omega = 0.2, T_r = 0.1, M_d = 2, G_h = 0.1, t = 2, R_e = 1, K_P = 1, H = 2$.

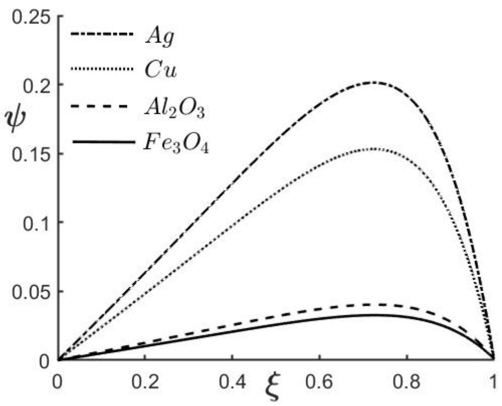

Figure 5 Velocity distribution of different nanoparticles in EG base fluids.

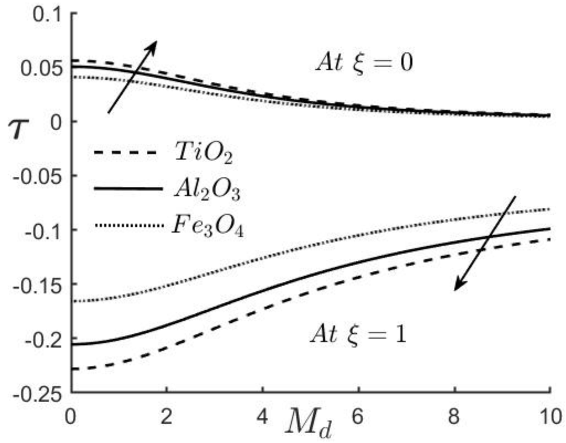

Figure 6 Skin friction distribution at $\xi = 0$ and $\xi = 1$ for various nanoparticles in EG base fluid.

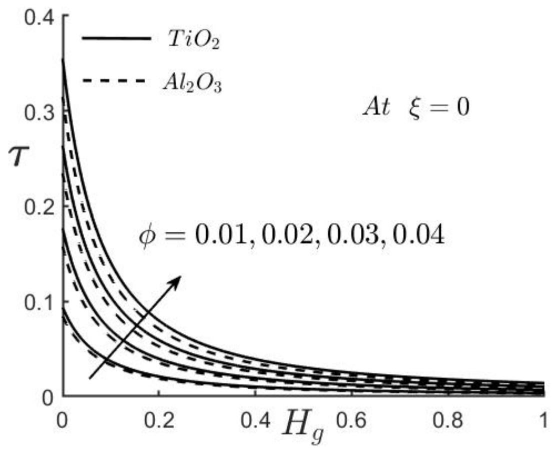

Figure 7 Variation of ϕ and H_g over the skin friction at $\xi = 0$.

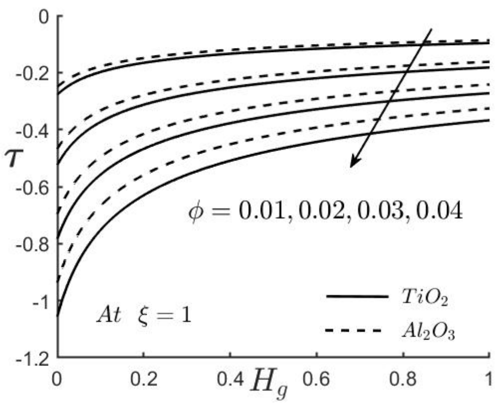

Figure 8 Variation of ϕ and H_g over the skin friction at $\xi = 1$.

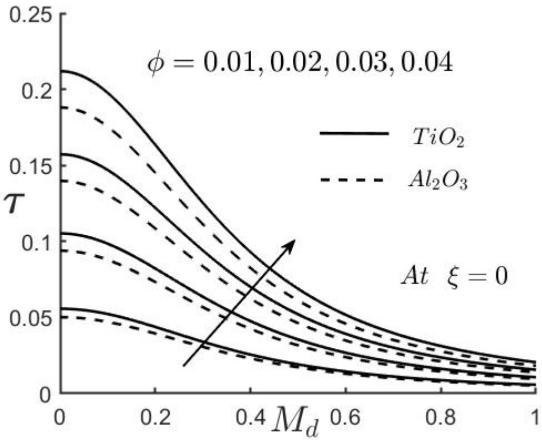

Figure 9 Variation of ϕ and M_d over the skin friction at $\xi = 0$.

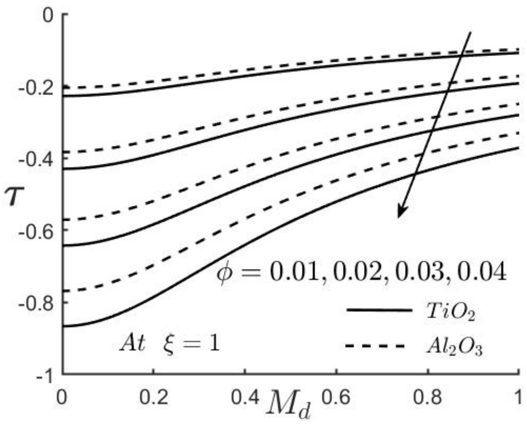

Figure 10 Variation of ϕ and M_d over the skin friction at $\xi = 1$.

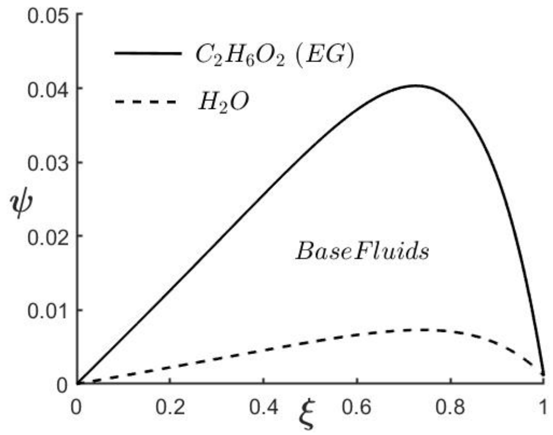

Figure 11 Comparison of base fluids over the velocity distribution of nanofluid**.**

Figure 5 depicts the behavior of various nanoparticles over the nanofluid velocity in the channel. Thermal conductivity is an important characteristic of nanofluid. When the thermal conductivity of the nanoparticles increases, heat transfer increases and particles move randomly from hot region towards cold. On the basis of higher density and thermal conductivity, the curves corresponding to Ag nanoparticle leads the higher numerical value over the nanoparticles Cu, Al_2O_3, Fe_3O_4 that means heat transfer occurs at higher rate in nano materials for higher thermal conductivity and therefore, more elevation has been detected in Ag and Cu nanoparticles. This shows that platelet shape Ag nanofluids has the highest viscosity and the thermal conductivity compared to Cu, Al_2O_3, Fe_3O_4 nanofluids which indicates that platelet shape Ag nanoparticle has better conductor quality. Materials of high thermal conductivity are widely used in heat sink applications.

Numerical values of the non-dimensional shear stresses at the plates $\xi = 0$ and $\xi = 1$ are presented in **Figure 6** for different platelet shape Nanoparticles. In engineering technology, the skin friction is useful in estimating not only the total frictional drag exerted on an object but also the convectional heat transfer rate on its surface. However, the positive or negative sign of τ, refers to the direction of the flow velocity. Due to higher viscosity and the thermal conductivity of Fe_3O_4, Al_2O_3 and TiO_2 nanoparticles, the shear stresses are elevated at the plate $y = 0$. However, opposite behaviour has been observed for Fe_3O_4, Al_2O_3 and TiO_2 nanoparticles at the plate $\xi = 1$ and all the values of τ are negative, which leads to back flow tendency of nanofluids.

The velocity gradients (i.e. skin friction, τ) at the plates $\xi = 0$ and $\xi = 1$ for various nanoparticles have been discussed for H_g and ϕ in **Figures 7** and **8** respectively. An increase in ϕ raises the skin friction near $\xi = 0$, but for $\phi > 0.04$ the profiles of τ are linear, this is due to less frictional effects of nanoparticles. Also at $\xi = 0$, increase in H_g reduces the values of τ for different values of ϕ. However, at the plate $\xi = 1$ all the effects of ϕ and H_g on τ are observed to be reversed compared to $\xi = 1$. Moreover, all the values of τ at the plate $\xi = 1$ are becomes negative for different ϕ and H_g, and it means that back flow of nanoparticles is occurred near the plate $\xi = 1$.

The impact of M_d and ϕ over the skin friction at the surfaces $\xi = 0$ and $\xi = 1$ in presence of Aluminium and Titanium dioxide are illustrated in **Figures 9** and **10** respectively. At the plate of rest (**Figure 9**), maximum elevation of τ is detected and away the plate it is least. The magnetic drag force due to Lorentz force resists the motion of the molecules, while the molecules are free to move for the effect of nanoparticle volume fraction. In physical point of view for the thermal conductivity, the curves corresponding to the TiO_2 attains at maximum numerical values than Al_2O_3. At the plate of oscillation (**Figure 10**), it is seen that the skin friction has an escalation for the impact of magnetic drag force, while a negative increasing of skin friction is observed for ϕ. Significantly, the behaviour of **Figure 9** is opposite to the **Figure 10**.

Figure 11 represents the behavior of base fluids over the velocity in the Couette flow motion. In the physical point of view, the density and thermal conductivity in Ethylene Glycol is heavier in comparison to water and therefore, less frictions are observed in water molecules that elevates the flow velocity of water rather than Ethylene Glycol (Hamilton and Crosser [15]).

The variations of nanoparticle volume fraction, thermal radiation, and heat generation over the temperature due to the impact of Al_2O_3 and TiO_2 in EG base nanofluids are shown in **Figures 12** and **13** for $\lambda = 0.5, \omega = 0.5, \Lambda = 0.52, T_r = 3, P_e = 1, H_g = 1$.

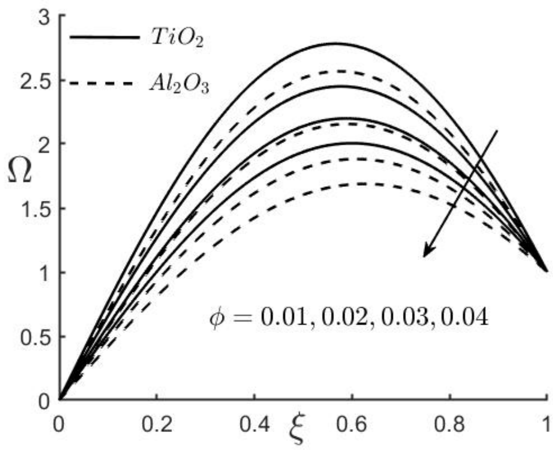

Figure 12 Effects of ϕ on temperature distribution in EG base fluid.

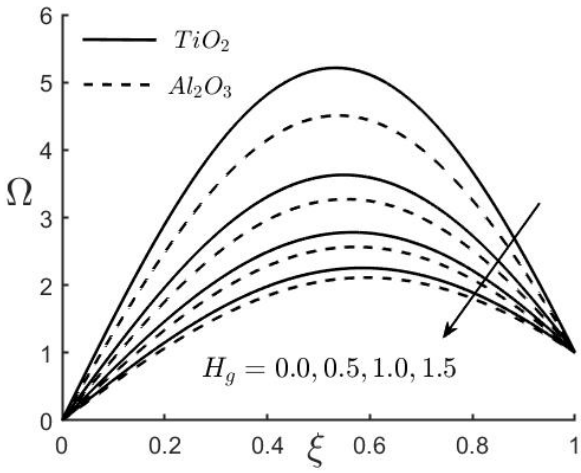

Figure 13 Effects of H_g on temperature distribution in EG base fluid.

The effect of nanoparticle volume fraction (ϕ) and heat generation (H_g) on temperature for the nanoparticles Al_2O_3 and TiO_2 in the EG base nanofluids is presented in **Figure 12** and **13** respectively. An increase in ϕ enhances the temperature of the nanofluid (**Figure 12**). In addition, the augmented ϕ enhanced the thermal conductivity increases, and thus reducing the thickness of thermal boundary layer. The TiO_2 nanoparticles exhibit higher temperature distribution than that of Al_2O_3 nanoparticles. This is because Al_2O_3 is more conductive metal than TiO_2. The augmented values of H_g decayed in the curves of temperature and its thickness of thermal boundary layers (**Figure 13**) in the channel. The thermal conductivity of a particular nanoparticle is highly dependent on the temperature gradient, nanoparticle properties, and the path length of nanoparticles carries heat. Therefore, when thermal conductivity is falling down from Al_2O_3 to TiO_2 nanoparticles, the lattice vibrations along with the free electrons are reduced which leads to degradation of temperature in both the **Figures 12** and **13**.

Conclusions

The significant outcomes on the impact of the Al_2O_3 and TiO_2 nanoparticles in EG base fluid due to the channel flow motion are highlighted below:

- The Lorentzian hydromagnetic drag forces impede strongly the boundary layer flow of nanoparticles, which serves as a potent control mechanism. Momentum boundary layer thickness is greatly reduced with strong magnetic field.
- A strong enhancement in velocity of Al_2O_3 and TiO_2 nanoparticles is generated with increasing ϕ and K values. Hence, momentum boundary layer thickness is therefore enhanced.
- Velocities and temperatures of nanofluids are also observed to be heavily depressed with strong heat generation ($H_g = 10.0$) as compared with an absence of heat generation ($H_g = 0$). Therefore, there is a significant reduction in momentum and thermal boundary layer thickness.
- $\phi = 0$, maximum elevation in temperature of nanofluids has been observed, while the temperature is almost linear for greater $\phi = 0.1$. This is due to heavy frictional forces of nanoparticles.
- In EG base fluids, shear stresses are more significant near $\xi = 0$ and $\xi = 1$ for both the effects of ϕ and H_g.
- In EG base fluids, platelet shape Ag - Cu Nanoparticles enhanced the velocity of nanofluids due to less viscosity and thermal conductivity.
- Shear stresses are quite effective near $\xi = 0$ and $\xi = 1$ when $\phi < 0.03$.
- Due to the impact of viscosity and thermal conductivity, all the velocity profiles of nanoparticles are highly elevated for TiO_2 over the Al_2O_3 Nanoparticles.

References

[1] SU Choi. Enhancing thermal conductivity of fluids with Nanoparticles. *Develop. Appl. Non-Newtonian Flows* 1995; **231**, 99-105.

[2] JC Maxwell. A Treatise on Electricity and Magnetism. Vol I, 3rd Ed. Oxford University Press, 1892.

[3] RA Mahdi, HA Mohammed, KM Munisamy and NH Saeid. Review of convection heat transfer and fluid flow in porous media with Nanofluid. *Renew. Sustain. Energ. Rev*., 2015; **41**, 715-34.

[4] R Nasrin, MA Alim and AJ Chamkha. Effect of the heating wall position on forced convection along two sided open enclosure with porous medium utilizing Nanofluid. *Int. J. Energ. Technol*. 2013; **5**, 1-13.

[5] W Ibrahim and BM Shankar. MHD boundary layer flow and heat transfer of a nanofluid past a permeable stretching sheet with velocity, thermal and solutal slip boundary conditions. *Comput. Fluids* 2013; **75**, 1-10.

[6] M Sheikholeslami, T Hayat and A Alsaedi. MHD free convection of Al_2O_3-water nanofluid considering thermal radiation: A numerical study. *Int. J. Heat Mass Transf*. 2016; **96**, 513-24.

[7] M Sheikholeslami, DD Ganji and MM Rashidi. Effect of non-uniform magnetic field on forced convection heat transfer of Fe_3O_4 - water nanofluid. *Comput. Meth. Appl. Mech. Eng.* 2015; **294**, 299-312.

[8] SE Awan, ZA Khan, M Awais, SU Rehman and MAZ Raja. Numerical treatment for hydro-magnetic unsteady channel flow of nanofluid with heat transfer. *Results Phys*. 2018; **9**, 1543-54.

[9] V Akula and S Srinivas. A study on hydromagnetic pulsating flow of a nanofluid in a porous channel with thermal radiation, *J. Mech*. 2016; **1**, 1-12.

[10] A Malvandi and DD Ganji. Effects of nanoparticle migration on hydromagnetic mixed convection of alumina/water nanofluid in vertical channels with asymmetric heating. *Physica E Low-Dimens. Syst. Nanostruct.* 2015; **66**, 181-96.

[11] M Sheikholeslami, M Hatami and DD Ganji. Analytical investigation of MHD nanofluid flow in a semi-porous channel. *Powder Technol.* 2013; **246**, 327-36.

[12] G Aaiza, I Khan and S Shafie. Energy transfer in mixed convection MHD flow of nanofluid containing different shapes of nanoparticles in a channel filled with saturated porous medium, *Nanoscale Res. Lett.* 2015; **10**, 490-503.

[13] SP Jang and SUS Choi. Effects of various parameters on nanofluid thermal conductivity. *J. Heat Transfer*. 2007; **129**, 617-23.

[14] B Widodo, DK Arif, D Aryany, N Asiyah, FA Widjajati and Kamiran. The effect of magnetohydrodynamic nanofluid flow through porous cylinder. *AIP Conf. Proc.* 2017; **2017**, 1867.

[15] RL Hamilton and OK Crosser. Thermal conductivity of heterogeneous two-component systems. *J. Indust. Eng. Chem. Fund*. 1962; **1**, 187-91.

[16] EV Timofeeva, RL Jules and S Dileep. Particle shape effect on thermophysical properties of alumina nanofluids. *J. Appl. Phys.* 2009; **106**, 01430.

[17] K Asma, I Khan and S Sharidan. Exact solutions for free convection flow of nanofluids with ramped wall temperature. *European Phys. J. Plus*. 2015; **130**, 57-71.

[18] G Aaiza, I Khan and S Shafie. Radiation and heat generation effects in magnetohydrodynamic mixed convection flow of nanofluids. *Thermal Sci*. 2018; **22**, 51-62.

[19] SMM EL-Kabeir, AJ Chamkha and AM Rashad. Effect of thermal radiation on non-darcy natural convection from a vertical cylinder embedded in a nanofluid porous media. *J. Porous Media* 2014; **17**, 269-78.

[20] D Kalita, S Hazarika and S Ahmed. Applications of CNTs in a vertical channel of porous medium for human blood flow: a rheological model. *JP J. Heat Mass Transfer*. 2020; **20**, 105-20.

[21] S Hazarika and S Ahmed. Study of carbon nanotubes with Casson fluid in a vertical channel of porous media for hydromagnetic drag force and diffusion-thermo. *J. Sci. Res*. 2021; **13**, 31-45.

[22] S Hazarika, S Ahmed and AJ Chamkha. Investigation of nanoparticles Cu, Ag and Fe_3O_4 on thermophoresis and viscous dissipation of MHD nanofluid over a stretching sheet in a porous regime: A numerical modeling. *Math. Comput. Simulat*. 2021; **182**, 819-37.
[23] S Hazarika, S Ahmed and SW Yao. Investigation of Cu-water nano-fluid of natural convection hydro-magnetic heat transport in a Darcian porous regime with diffusion-thermo. *Appl. Nanosci*. 2021. https://doi.org/10.1007/s13204-020-01655-w.
[24] L Colla, L Fedele, M Scattolini and S Bobbo. Water-based Fe_2O_3 nanofluid characterization: thermal conductivity and viscosity measurements and correlation. *Adv. Mech. Eng*. 2012; **8**, 674947.
[25] T Armaghani, A Kasaeipoor, N Alavi and MM Rashidi. Numerical investigation of water-alumina nanofluid natural convection heat transfer and entropy generation in a baffled L-shaped cavity. *J. Molecular Liquids* 2016; **223**, 243-51.
[26] AJ Chamkha, AM Rashad, MA Mansour, T Armaghani and M Ghalambaz. Effects of heat sink and source and entropy generation on MHD mixed convection of a Cu-water nanofluid in a lid-driven square porous enclosure with partial slip. *Phys. Fluids* 2017; **29**, 052001.
[27] M Molana, AS Dogonchi, T Armaghani, Ali J Chamkha, DD Ganji and I Tlili. Investigation of hydrothermal behavior of Fe3O4-H2O nanofluid natural convection in a novel shape of porous cavity subjected to magnetic field dependent (MFD) viscosity. *J. Energ. Storage*. 2020; **30**, 101395
[28] T Armaghani, AJ Chamkha and M Ishmael. Analysis of entropy generation and natural convection in an inclined partially porous layered cavity filled with a nanofluid. *Canadian J. Phys.* 2016; **95**, 238-52.
[29] AM Rashad, AJ Chamkha, MA Ismael and T Salah. Magnetohydrodynamics natural convection in a triangular cavity filled with a Cu-Al_2O_3/water hybrid nanofluid with localized heating from below and internal heat generation. *Heat Transfer* 2018; **140**, 072502.
[30] S Jakeer, PB Reddy and HA Nabwey. Impact of heated obstacle position on magneto-hybrid nanofluid flow in a lid-driven porous cavity with Cattaneo-Christov heat flux pattern. *Alexendria Eng. J.* 2021; **60**, 821-35.
[31] EREL Zahar, AM Rashad, W Saad and LF Seddek . Magneto-hybrid nanofluids flow via mixed convection past a radiative circular cylinder. *Scientific Reports* 2020; **10**, 10494.
[32] M Ghalambaz and AH Veismoradi. Unsteady natural convection flow of a suspension comprising Nano-Encapsulated Phase Change Materials (NEPCMs) in a porous medium. *Adv. Powder Tech*. 2020; **31**, 954-66.
[33] SMH Zadeh, SAM Mehryan, M Sheremet, M Ghodrat and M Ghalambaz. Thermo-hydrodynamic and entropy generation analysis of a dilute aqueous suspension enhanced with nano-encapsulated phase change material. *Int. J. Mech. Sci*. 2020; **178**, 105609.
[34] H Darcy. *Les Fontaines Publiques de la ville de Dijon*. Dalmont, Paris, 1856.
[35] J Hartmann. Hg-dynamics-I, theory of the laminar flow of an electrically conducting liquid in a homogeneous magnetic field, Kgl, Danske Videnskab. *Selskab Mat-Fys. Medd.* 1937; **15**, 1-28.

Nomenclature

$\overline{\psi}$	dimensional nanofluid velocity in $\overline{\zeta}$-direction, m/s	Λ	sphericity of nanoparticles
$\overline{\chi}$	dimensional nanofluid velocity in $\overline{\xi}$-direction, m/s	ε	reference constant for perturbation
$\overline{\Omega}$	dimensional temperature, K	a and b	constants and depend on the particle shape
ψ	non- dimensional nanofluid velocity	d	distance between the wall of the channel, m
Ω	non- dimensional nanofluid tempearture	g	acceleration due to gravity, m/s^2
Ω_0	nanofluid temperature at $\overline{\xi} = 0$	G_h	Grashof number
Ω_w	nanofluid temperature at $\overline{\xi} = d$	H_g	dimensionless heat generation parameter
$(\overline{\zeta}, \overline{\xi})$	chosen Cartesian coordinate of the channel	$\overline{K}_1$	permeability of the porous medium
ρ_{nf}	density of nanofluids, kg/m^3	K_P	porosity parameter
μ_{nf}	dynamic viscosity of nanofluid, kg·m^{-1}·s^{-1}	M_d	magnetic parameter
σ	electrical conductivity of base fluid, Sm^{-1}	n	empirical shape factor
$(\rho\beta)_{nf}$	thermal expansion coefficient of nanofluids, kg/(K.m^3)	p	pressure, kg·m^{-1}·s^{-2}
$(\rho C_p)_{nf}$	heat capacitance of the nanofluids, J/K	P_e	Peclet number
κ_{nf}	thermal conductivity of nanofluids, W/(m.K)	Q_g	dimensional heat generation parameter
ϕ	nanoparticles volume fraction,	R_e	Reynolds number
ρ_f and ρ_s	densities of the base fluid and solid nanoparticles, kg/m^3	$\overline{t}$	time, s
β_f and β_s	volumetric coefficients of thermal expansions of solid nanoparticles and base fluids	$\overline{T}_r$	radiative heat flux in $\overline{\zeta}$-direction
$(C_p)_s$ and $(C_p)_f$	specific heat capacities of solid nanoparticles and base fluids at constant pressure	T_r	radiation parameter
α	radiation absorption coefficient		

Appendix

$$\left\{\begin{array}{c} \phi_1 = (1-\phi) + \phi\dfrac{\rho_s}{\rho_f}, \ \ \phi_2 = 1 + a\phi + b\phi^2, \ \ \phi_3 = (1-\phi) + \phi\dfrac{(\rho\beta)_s}{(\rho\beta)_f}, \ \ \lambda_1 = \dfrac{\lambda}{\phi_2}, \\ \phi_4 = (1-\phi) + \phi\dfrac{(\rho C_p)_s}{(\rho C_p)_f}, \ \ a_0 = \phi_1 Re, \ \ m_0^2 = M_d^2 + \dfrac{\phi_2}{K}, \ \ a_1 = \phi_3 G_h, a_2 = \dfrac{a_1}{\phi_2}, \\ b_0^2 = \phi_4 Pe\dfrac{1}{\lambda_n}, \ \ b_1^2 = \dfrac{T_h^2}{\lambda_n}, b_2^2 = b_1^2 - H_g, b_3^2 = b_2^2 - i\omega\, b_0^2, \ \ m_1^2 = \dfrac{m_0^2}{\phi_2}, \ \ m_2^2 = \dfrac{m_0^2 + a_0 i\omega}{\phi_2} \end{array}\right\}$$